Improved Fine Sun Sensor Field of View Calibration*

J. Sedlak and J. Hashmall
Computer Sciences Corporation
Lanham-Seabrook, Maryland, USA 20706

Abstract

The fine Sun sensor used on many spacecraft consists of two independent single-axis sensor heads, nominally mounted perpendicularly. These detect the Sun angle over a field of view typically of ±32 deg. (There is a trade-off between accuracy and size of the field of view that allows for much latitude in any numbers quoted.) The nonlinear "transfer" function that maps the telemetered counts into observed angles consists of 9 adjustable parameters for each axis (18 total). An augmented transfer function has previously been reported that achieves a significant accuracy improvement across the entire field of view. That function expands the parameter set to 12 coefficients per axis (24 total) and includes cross terms combining counts from both axes.

To make the best use of the Sun sensor for attitude determination, it must be calibrated after launch. However, the large number of parameters and the nonlinearity of the problem make this a challenging task. The purpose of this paper is to examine ways to improve convergence of the parameter search algorithm. In particular, experience has shown that the problem should be broken down into several steps, solving for a selected subset of the parameters at each step. This approach has now been incorporated as an option in the calibration utility.

INTRODUCTION

Digital Sun sensors are often used onboard spacecraft to measure the direction of the Sun for use in attitude determination and control. The fine Sun sensor (FSS) design combines a digital sensor with an analog component to improve the observation accuracy to 1 arcmin or better. The sensor data in the examples in this paper come from the FSSs manufactured by Adcole for the Upper Atmosphere Research Satellite (UARS) and the Rossi X-Ray Timing Explorer (RXTE). This paper reviews the nonlinear transfer function used to convert the telemetered FSS counts into Sun angle observations and discusses the calibration process needed to improve the transfer function coefficients after launch (referred to here as field of view (FOV) calibration). Experience gained from tests with flight data and simulations shows it is often difficult to find the optimal solution for the FOV calibration. This paper examines procedural steps that have been found to help locate the solution for this multi-parameter problem. The procedure has now been incorporated explicitly in the calibration software and gives the analyst an option to automatically break down the parameter search into multiple steps, greatly increasing the likelihood of convergence.

Usually two sensor heads are combined to measure the Sun angle about orthogonal axes, which together define the Sun unit vector in the sensor frame. For the digital sensor, each head has an entrance slit that passes a wedge of sunlight through to a mask having a pattern of slits, and through that to an array of photocells. The angle of the wedge of sunlight determines which slits are illuminated, and thus, which photocells are powered. Each unique combination of powered photocells corresponds to an observed Sun angle (usually Gray coded).

---

* This work was supported by the National Aeronautics and Space Administration (NASA) / Goddard Space Flight Center (GSFC), Greenbelt, MD, USA, Contract GS-35F-4381G, Task Order no. S-71002-G.

NASA/GSFC, Mission Engineering and Systems Analysis Division, *Flight Mechanics Symposium*, Greenbelt, MD, Oct. 2003.

The accuracy of this digital sensor design is limited by the finite angular diameter of Sun, which is 0.53 deg at the distance of the Earth. This limits how fine the least-significant bit slit pattern can be before signals from adjacent bits can no longer be distinguished. The FSS achieves much greater accuracy by employing a double mask detector, discussed below.

The FSS transfer function provided by the manufacturer consists of 9 parameters for each sensor head. The work described in Ref. 1 introduced 3 new parameters for each head and accounted for coupling between the two axes. The use of this larger set of coefficients improved the accuracy to 15 arcsec (1σ) over the entire FOV but made it still more difficult to obtain a good calibration solution.

The next section of this paper reviews the FSS transfer function in its basic and expanded forms and discusses the role of each coefficient. A geometric interpretation is given for each of the 3 new coefficients in the expanded function. The following section on software enhancements discusses a simple calibration procedure for estimating improvements to the coefficients. The procedure involves several steps where the parameters are estimated in their order of importance. The final sections give test results and conclusions. The tests verify that the improved calibration software does converge reliably to determine the correct coefficients using both simulated and flight data.

TRANSFER FUNCTION

Background

Detailed descriptions of Sun sensors and their mathematical models can be found in Ref. 2. The background information reviewed here touches on only a small part of this material.

The Sun unit vector in the sensor frame is given by

$$\begin{bmatrix} X \\ Y \\ Z \end{bmatrix} = \left(1 + \tan^2\alpha + \tan^2\beta\right)^{-1/2} \begin{bmatrix} \tan\alpha \\ \tan\beta \\ 1 \end{bmatrix} \tag{1}$$

where α and β are the dihedral angles of the Sun vector about the sensor Y- and X-axes, respectively. That is, they are the angles from the sensor boresight (Z-axis) to the projection of the Sun on the X–Z and Y–Z planes, respectively. (This is the definition from the software specifications in Ref. 3, and differs from Ref. 2.) It is assumed that the sensor axes are orthogonal. If there is any nonorthogonality, it can be corrected in the calibration process, as discussed below.

The actual sensor measurements are provided in telemetry as counts, N_α and N_β. These are converted to the α and β angles using the transfer function

$$\alpha = \arctan\left[A_1 + A_2 N_\alpha + A_3 \sin\left(A_4 N_\alpha + A_5\right) + A_6 \sin\left(A_7 N_\alpha + A_8\right)\right] + A_9 \tag{2a}$$

$$\beta = \arctan\left[B_1 + B_2 N_\beta + B_3 \sin\left(B_4 N_\beta + B_5\right) + B_6 \sin\left(B_7 N_\beta + B_8\right)\right] + B_9 \tag{2b}$$

The expanded transfer function presented in Ref. 1 modifies α and β, as follows

$$\alpha' = \alpha + A_{10} + A_{11}\beta + A_{12}\alpha\beta \tag{3a}$$

$$\beta' = \beta + B_{10} + B_{11}\alpha + B_{12}\alpha\beta \tag{3b}$$

This particular augmentation of the transfer function was selected empirically from about 20 candidate functions in tests using a large volume of data from the UARS spacecraft. It introduces only 3 new parameters on each axis while still providing significant improvement to the sensor accuracy.

The FOV calibration (Ref. 3) consists of varying the values of the A_n and B_n coefficients to minimize a loss function constructed from the sum of the squares of the Sun residuals (that is, observations minus reference vectors expressed in a common frame).

In the following discussion, the counts N_α and N_β will be referred to generically as N, and any comments about α and A_n apply equally to β and B_n unless otherwise noted.

The coefficients A_1 and A_2 are the bias and scale factor for the counts N. The parameter A_9 provides a bias for the α angle directly. For small angles, A_1 and A_9 are nearly indistinguishable. Data samples over a large part of the FOV are needed to determine these coefficients separately.

Figure 1 shows the range of values of tan(α) from Eq. 2 over the full range of counts for the Adcole FSS used on UARS. The function is dominated by the linear term. This makes A_1 and A_2 the most easily determined coefficients.

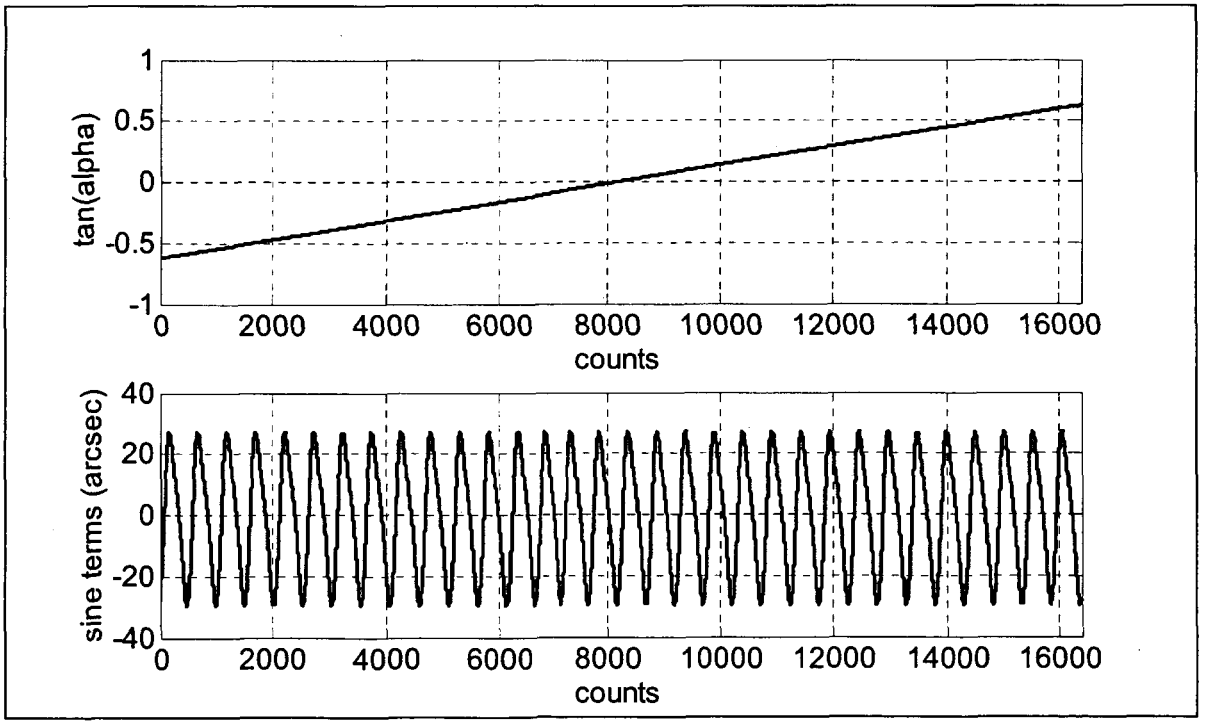

Fig. 1. Range of tan(α) for full range of counts for the UARS FSS; lower curve shows only the sinusoidal terms with amplitudes A_3 and A_6 expressed in arcsec.

In the lower part of Figure 1, the constant and linear terms have been subtracted from $\tan(\alpha)$ to show just the sinusoidal terms with amplitudes A_3 and A_6. These terms are unique to the fine Sun sensor (as distinct from an ordinary digital Sun sensor). Their amplitudes amount to about a ± 30 arcsec variation around the linear term. This is small enough so that the slope of the $\tan(\alpha)$ curve never changes sign, and the mapping from counts to angles remains one-to-one; however, it is large enough to provide the needed Sun angle correction.

The sinusoidal terms are produced by combining signals from a double mask detector. The two masks have different numbers of slits, so the Sun illumination on the photocells varies periodically with incidence angle (see Ref. 2 for details). There are four such sets of masks, with slits positioned so the periodic output of each is offset by 90 deg phase from the next. These four signals are combined electronically to produce the pattern in Figure 1. For the Adcole FSS on UARS, the resulting values for α and β have 14 arcsec resolution (least significant bit), while the overall accuracy is specified to be 60 arcsec within a circular FOV of 32 deg radius.

It was noticed that, using only the 9 coefficients for each axis as in Eqs. 2, the distribution of errors was not uniform over the FOV. As described in Ref. 1, it was possible to account for the systematic error by introducing additional coefficients as in Eqs. 3. This achieved a root-mean-square accuracy of about 15 arcsec. Similar accuracy was achieved for the FSS on RXTE, although the initial errors were not so large (Ref. 4). Reference 5 gives a review of calibration results for a number of missions.

Analysis

This section discusses a number of ways to simplify the search for improved coefficients. Most of these have been implemented to improve convergence in the FOV calibration software discussed in the next section. Any reduction in the dimensionality of the search space can help make the minimization algorithm converge more reliably.

One simplification is to set A_9 and B_9 to zero after first performing an independent sensor alignment calibration. Alignment calibration consists of estimating an orthogonal transformation to correct the sensor alignment relative to the body frame (Refs. 3 and 6). The alignment corrections around the X- and Y-axes are closely related to the A_9 and B_9 FOV corrections. (That they are not identical can be seen by considering a rotation about the X-axis. This has no effect on the X-component of the observation vector, but a change in A_9 affects all 3 components through the normalization factor in Eq. 1.) It is important that both the FOV and alignment calibrations make use of data over the entire FOV to avoid bias due to any asymmetric sensor response. If mission constraints limit the Sun to a restricted part of the FOV, the calibrations should use just this part.

If A_9 and B_9 are not solved for, then A_1 and B_1 can be more easily found. After the other coefficients are determined, A_9 and B_9 can be reintroduced and estimated as a small additional correction to the alignment, if desired.

The second simplification is to note that the nominal periodicity of the second sinusoidal term is exactly twice that of the first; that is, $A_7 = 2A_4$. This arises from the Fourier series representation of the output from the slits in the ideal sensor, carrying the expansions one order higher than those given in Ref. 2. One can optionally restrict A_7 to be twice A_4 while solving for first estimates of the other coefficients, then repeat the calibration, allowing A_7 to vary independently to account for deviations of the sensor geometry from ideal. If good initial guesses for A_4 and A_7

are not known, they can be the most difficult parameters to estimate. Future work will look at ways to determine these frequencies, possibly using an integral transform, although this is complicated by the unknown and uneven distribution of the α and β data.

The new coefficients A_{10}, A_{11}, and A_{12} all have geometric interpretations. The A_{10} term is a bias for the corrected angle α'. It is almost indistinguishable from the bias A_9, the only difference coming from 2nd-order contributions in combination with A_{11} and A_{12}. The A_{11} and B_{11} terms are the most important of the new parameters. They must be discussed together since they couple the α and β measurements. Combined with the leading-order term from Eqs. 3, their effect can be written as

$$\begin{bmatrix} \alpha' \\ \beta' \end{bmatrix} = \begin{bmatrix} 1 & A_{11} \\ B_{11} & 1 \end{bmatrix} \begin{bmatrix} \alpha \\ \beta \end{bmatrix} \tag{4}$$

If $A_{11} = -B_{11} \approx \sin(\vartheta)$, Eq. 4 would represent a simple rotation in the (α, β)-plane by the small angle ϑ ($\cos(\vartheta) \approx 1$). For small α and β, this is the same as an alignment correction around the sensor boresight. Even for large α and β, the effect of Eq. 4 is nearly the same as a true orthogonal rotation; for example, the difference in the resulting Sun observation vectors as given by Eq. 1 is less than 2×10^{-4} over the entire FOV for $\vartheta = 0.1$ deg.

The conclusion here is that one can take $A_{11} = B_{11}$ after having first performed an alignment calibration. After obtaining first estimates for the other FOV coefficients, one can repeat the calibration, allowing A_{11} and B_{11} to vary independently to absorb any remaining misalignment.

There is a different interpretation when $A_{11} = B_{11} \approx \sin(\varphi/2)$. In this case, Eq. 4 represents a skew transformation as shown in Figure 2. This provides an approximate correction for errors

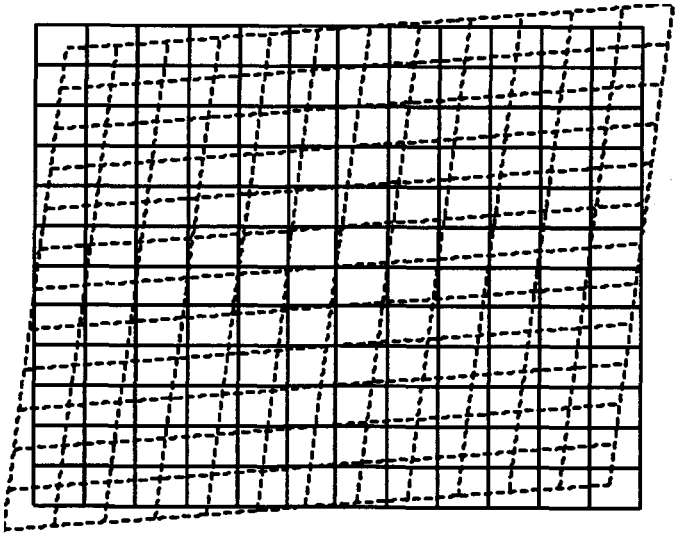

Fig. 2. Skew error corrected by coefficient A_{11} (and $B_{11} = A_{11}$); the α and β coordinate grid is shown as solid lines and the α' and β' coordinate grid as dashed lines.

caused by the α and β heads not being mounted at exactly 90 deg. This can be a very important correction since the alignment calibration software currently used operationally at the Goddard Space Flight Center (GSFC) always assumes the axes are physically orthogonal.

In general, one can interpret A_{11} and B_{11} as representing a boresight rotation angle of $\vartheta \approx (A_{11} - B_{11})/2$ and a total skew angle of $\varphi \approx (A_{11} + B_{11})$, where each axis is skewed by $\varphi/2$.

The A_{12} and B_{12} corrections provide a nonlinear transformation that corresponds to a compression distortion in one half-plane and an expansion in the other half-plane. The correction is zero on the α and β axes; e.g., $\alpha' = \alpha$ when $\beta = 0$, and $\beta' = \beta$ when $\alpha = 0$. An exaggerated example is shown in Figure 3 for the case $A_{12} = 0.3$ and $B_{12} = 0.3$, showing the distortion over the entire FOV. It is possible that this type of distortion could arise from noncoplanarity of the two masks and the photocells.

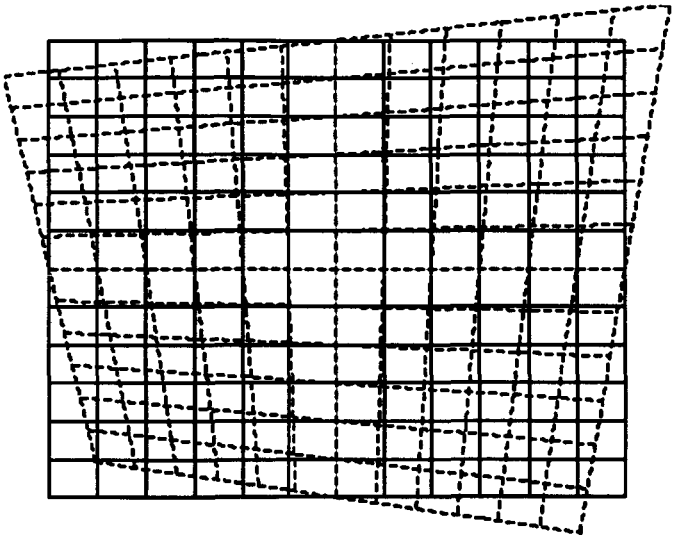

Fig. 3. Distortion corrected by coefficients A_{12} and B_{12}; the α and β coordinate grid is shown as solid lines and the α' and β' coordinate grid as dashed lines.

The boresight direction is defined as the origin in the (α', β') plane. The A_{10} and B_{10} coefficients are simple biases for α' and β', so they shift the coordinate grid and move the center of the distortion pattern seen in Figure 3 away from the boresight. On the other hand, A_9 and B_9 also shift the boresight (like an alignment calibration), but the center of the distortion pattern moves with it. Again, it is clear that if A_{12} and B_{12} are near zero, the biases from coefficients 9 and 10 become indistinguishable and should not both be included in the search.

SOFTWARE IMPROVEMENTS

The FOV calibration utility is implemented as a subsystem of the Flight Dynamics Ground Support System (Ref. 3) using the MATLAB® (The MathWorks, Inc.) programming environment. All the user options and parameters are initialized through a namelist file and can be modified through a graphical user interface. As mentioned above, the calibration proceeds by

varying the A_n and B_n coefficients to minimize the sum of the squares of the observation residuals. When executed, the utility calls a MATLAB minimization routine that uses a simplex method. This replaces an earlier version that used the Levenberg-Marquardt algorithm.

Table 1 shows approximate values or typical magnitudes for the 12 coefficients. These values range over 5 orders of magnitude. An option has been added to the calibration utility to scale all the coefficients to be of order unity before calling the MATLAB minimizer. If this option is selected, the user can input the scaling factors or use internal hard-coded values. This improves the search, particularly in the first few iterations.

Table 1. Typical values for the A_n and B_n coefficients.

Coefficient	Typical Value	Units
1	-0.62	-
2	7.6×10^{-5}	1/counts
3	2×10^{-5}	-
4	0.012	rad/count
5	Arbitrary (0-2π)	rad
6	1×10^{-5}	-
7	0.024	rad/count
8	Arbitrary (0-2π)	rad
9	$\lesssim 10^{-3}$	rad
10	$\lesssim 10^{-3}$	rad
11	$\lesssim 10^{-3}$	-
12	$\lesssim 10^{-3}$	1/rad

There also is a wide range in the precisions with which the coefficients are known. The constant and linear terms (A_1 and A_2) must be known to 4-5 significant digits to represent angles with an accuracy of 60 arcmin and least significant bit of 15 arcsec. The amplitudes (A_3 and A_6) together contribute a correction of only 30 arcsec (Figure 1), so they can be determined only to 1-2 digits. The periodicities of the sinusoids (A_4 and A_7) are fairly well known a priori from the slit spacing and geometry—they can be determined to 3-4 significant digits given sufficient data. However, if good initial estimates for these are not available, it becomes much more difficult to obtain a good calibration solution.

It should be possible to determine the biases (A_9 and A_{10}) with a combined absolute error of about 15 arcsec, but there may be much larger correlated errors in each that tend to cancel. The skew and distortion terms (A_{11} and A_{12}) are expected to be small corrections; only their leading 1-2 digits will be significant. The phase coefficients (A_5 and A_8) have been found to be difficult to estimate and probably can be determined only to 2 significant digits. They require that the FOV be well sampled.

The user can select any subset of the 12 coefficients as solve-for parameters. However, if all 12 are selected, it is very unlikely that the algorithm will converge unless the initial guesses are

already very close to a solution. For this reason, the experienced analyst will solve the problem in steps, selecting the most important coefficients first. This reduces the size of the search space for the minimization problem that must be solved numerically at each step.

An option to perform the calibration in multiple steps has now been incorporated in the FOV calibration utility. This attempts to automate the procedure used by the experienced analyst. The specific steps for estimating the A_n (and the B_n) coefficients are:

1. Solve for the constant and linear terms, A_1 and A_2
2. Solve for the bias, A_9
3. Solve for the first sinusoidal term, A_3, A_4 and A_5
4. Solve for the second sinusoidal term, A_6, A_7, and A_8
5. Solve for the augmented transfer function parameters, A_{10}, A_{11}, and A_{12}
6. Repeat the estimation of the phases, A_5 and A_8
7. Repeat the estimation of the frequencies, A_4 and A_7
8. Repeat the estimation of the set, A_1, A_2, A_3, A_6, A_{10}, A_{11}, and A_{12}

The phase terms are not repeated in the last step because they have already been estimated twice in steps 2, 3, and 4. The periodicity terms, A_4 and A_7, are not included in the last step because they should already be fairly well determined—the estimated value of the spatial frequency will not change due to correlations with other parameters. If the frequencies and phases have not been determined accurately, oscillations will show up in the residuals plots. In this case, the calibration should be iterated.

The user can select a subset of the 12 parameters and still use the multiple step option. The software will perform a subset of the 8 steps, as appropriate. There also is an option to force A_7 to be exactly twice A_4 for all steps.

After performing the multi-step calibration, the user can attempt to solve for all the selected parameters together in a single step. At that stage, the estimates may be accurate enough so the search will converge. In the tests, though, it was more useful to limit this optional step to solve only for improvements to the sinusoidal coefficients, A_3 through A_8. These are difficult to estimate and yet are necessary to take advantage of the FSS design. The most serious remaining problem with both the single step and the automated multi-step method is the difficulty of determining coefficients 3 through 8 when the initial guesses are not close enough.

TEST RESULTS

A number of tests have been performed to validate the improved FOV calibration software. These tests have used simulated data and flight data from UARS. For the simulations, the FSS coefficients were taken from either RXTE or UARS and were artificially corrupted to challenge the software with known errors.

Test 1

The first test simulated a scenario where the spacecraft was maneuvered in 7 steps of 10 deg each about the α and β Sun sensor axes. This provided 49 groups of Sun observations with the Sun positioned on a grid of 49 locations in the FOV. The angles ranged from –30 to +30 deg

about α and β. The measurements were taken once per second for about 100 seconds at each Sun location. The truth model coefficients were similar to those from RXTE, but with $A_{10} = 0$ and $A_7 = 2A_4$. The corrupted coefficients had randomly chosen errors varying from the truth values by 5 percent (1σ). This gave the initial α and β residuals a mean value of 5 deg and a standard deviation of 1 deg (these are the root-sum-squares (RSS) of the α and β residuals' means and standard deviations). These errors are much larger than what one would expect to find during the initial post-launch calibration. However, most of this initial error was due to coefficients A_1 and A_2 only. The multi-step method removed almost all of the error in the first step and gave only small improvements in the subsequent steps. The final residuals had a mean value of zero.

This test scenario was repeated with varying amounts of error added to the initial parameters. It was found that the leading coefficients, the biases, and the skew and distortion terms could be determined without difficulty (contributing α and β errors under 1 arcsec RSS), but the estimated values for the sinusoidal terms were very unreliable (causing RSS standard deviations ranging from 3 to 20 arcsec). Errors of this size would be acceptable in an actual flight scenario but are too large for a simulation where there are no other unaccounted for systematic or random error sources. This shortcoming is addressed in the next test.

Test 2

The second test scenario attempted to improve the observability by stepping the Sun across the FOV in small steps of 0.1 deg rather than grouping the observations in clusters. The Sun was swept across the FOV three times in the α direction while varying the β value, and three times in the β direction while varying α. This greatly improved the sampling of the oscillations shown in Figure 1. This test started with the UARS parameters, and coefficients 1, 2, 3, 6, 9, 11, and 12 again were corrupted by adding random values varying from the truth values by 5 percent (1σ). The spatial frequencies, A_4 and A_7, were varied by 2 percent, and the phases by 30 deg.

In this case, all the coefficients could be determined accurately. The remaining errors in the coefficients, compared to the truth values, gave α and β standard deviations that were all under about 1 arcsec. However, if the frequencies were corrupted by 5 percent, the minimizer often failed to lock in on the correct values.

Test 3

The third test case used UARS flight data from 5 different days during a time span of 6 weeks. UARS is an Earth-oriented spacecraft, so the Sun usually passes through the FSS FOV once each orbit. Due to the precession of the orbit plane, the path of the Sun through the FOV shifts with time. This makes the observability very good for β and at least fair for α.

The UARS pre-calibration residuals had a mean value of 41 arcsec and a standard deviation of 47 arcsec (RSS of α and β). The multi-step calibration was run first with just the first 8 coefficients. This brought the residuals down to a mean of 1 arcsec but did not improve the standard deviation. The second iteration solved for all but coefficients 6, 7, 8, and 9. This reduced the standard deviation to 19 arcsec. Further iterations to find a better fit to the sinusoidal terms did not improve the results even though the residuals plots still showed significant oscillations. It is likely that the estimator could not remove all the oscillations because the onboard attitude being used to transform the reference Sun into the body frame was accurate only to about 20 arcsec.

CONCLUSIONS

The main purpose of this work has been to analyze and improve the current software for calibrating the FOV correction parameters for fine Sun sensors. After reviewing the FSS transfer function, a geometric interpretation was given for each of the 3 new coefficients in the expanded form. This analysis motivated incorporating into the calibration software options to combine or eliminate some of the coefficients. Other new features in the calibration software include:

- Option for scaling the coefficients internally to the loss function minimization routine so the typical values of all coefficients are of order unity.
- Option to solve for the loss function global minimum in multiple steps, where each step deals only with a subset of the coefficients. The coefficients are determined in their order of importance. This imitates the manual approach used by experienced analysts working with actual flight data.
- Minor improvements to the input/output and user interface.

Test results were presented to show that the improved calibration software converges reliably to determine the correct coefficients, as long as the a priori values for the frequencies of the sinusoidal terms were within about 2 percent of the truth values. The test cases used both simulated data and flight data from UARS. The attitude uncertainty in the flight data was a source of noise that limited the accuracy of the solution. In spite of this, the resulting accuracy was 19 arcsec (1σ), which is much better than the 60 arcsec specification for the FSS.

The software enhancements provide a more robust method of solution for this highly non-linear minimization problem. The resulting calibration utility yields better calibration solutions with less analyst effort. Additional improvements to the procedure may be possible that would make the convergence still more reliable over a wider range of initial parameter values. In particular, future work will look at alternative ways to determine the spatial frequencies.

REFERENCES

1. J. Hashmall and D. Baker, "An Improved Transfer Function for the Fine Sun Sensor," *Proc. of the Int. Symp. on Space Flight Dynamics*, St. Petersburg and Moscow, Russia, sponsored by the Keldysh Inst. of Appl. Math. and the Space Research Inst. of the Russian Acad. of Sciences and the Russian Space Agency, May 1994.
2. J. R. Wertz (ed.), *Spacecraft Attitude Determination and Control*, D. Reidel Publishing Company, Dordrecht, The Netherlands, 1978.
3. J. Landis, et al., "Multimission Three-Axis Stabilized Spacecraft (MTASS) Flight Dynamics Support System Functional Specifications, Rev.1," Computer Sciences Corporation, prepared for NASA/GSFC, 554-FDD-91/070R1UD0, CSC/TR-91/6071R1UD0, September 1995.
4. D. Fink, et al., "Rossi X-Ray Timing Explorer (RXTE) Postlaunch Report," Computer Sciences Corporation, prepared for NASA/GSFC, 553-FDD-96/005R0UD0, CSC-10032526, June 1996.
5. J. Hashmall, J. Rowe, and J. Sedlak, "Spacecraft Attitude Sensor Calibration from On-Orbit Experience," *AIAA/IEEE 16th Digital Avionics Systems Conference*, Irvine, CA, Oct. 1997.
6. J. Hashmall and J. Sedlak, "New Attitude Sensor Alignment Calibration Algorithms," *Int. Astronautical Congress*, Houston, TX, Oct. 2002.